

Absence of gapped broken inversion symmetry phase of electrons in bilayer graphene under renormalized-ring-diagram approximation

Xin-Zhong Yan¹ and C. S. Ting²

¹*Institute of Physics, Chinese Academy of Sciences, P.O. Box 603, Beijing 100190, China*

²*Department of Physics, University of Houston, Houston, Texas 77204, USA*

(Dated: March 20, 2019)

On a lattice model, we study the possible existence of gapped broken inversion symmetry phase (GBISP) of electrons with long-range Coulomb interactions in bilayer graphene using both self-consistent Hartree-Fock approximation (SCHFA) and the renormalized-ring-diagram approximation (RRDA). RRDA takes into account the charge-density fluctuations beyond SCHFA. Although GBISP at low temperature and low carrier concentration is predicted by SCHFA, we show here that this state can be substantially suppressed by the charge-density fluctuations in RRDA. We also present a numerical algorithm for calculating the self-energy of electrons with the singular long-range Coulomb interaction on the lattice model.

PACS numbers: 71.10.-w, 71.10.Fd, 73.22.Pr, 71.15.Dx

I. INTRODUCTION

Bilayer graphene, because of its controllable band gap by external gate voltage, is a promising candidate for application in electronic devices.¹⁻⁴ In the low carrier doping regime, electrons in bilayer graphene are strongly coupled via the Coulomb interactions. One of the fundamental problems is the phase of the system at low carrier concentration and low temperature. Several candidates for the ground state, such as the gapped ones including ferroelectric-layer asymmetric state,⁵⁻⁹ layer polarized antiferromagnetic state,^{10,11} quantum anomalous Hall,^{8,12,13} quantum spin Hall,^{8,13} quantum valley Hall,¹⁴ charge density wave,¹⁵ as well as the gapless nematic state^{16,17} have been discussed in recent literatures. The experimental observations on the ground state are also controversial. Some results showed that the state is gapped at the neutrality point,¹⁸⁻²¹ while one experiment found a gapless state.²² So far, most of the theoretical studies are based on the self-consistent Hartree-Fock approximation (SCHFA),^{5,9,14} the perturbation theory,⁷ and the renormalization group approaches^{11,16,17} on simplified two-band continuous model. It is well known that SCHFA usually overestimates the order parameter characterizing a broken symmetry state and the transition temperature because it neglects the field fluctuation. Because the understanding of the relevant electronic state at low carrier doping and low temperature is a fundamental issue for the application of bilayer graphene, it is necessary to investigate the state with a sophisticated approach that takes into account the effect due to charge density fluctuations.

In this work, we study the existence of gapped broken inversion-symmetry phase (GBISP) using both SCHFA and the renormalized-ring-diagram approximation (RRDA) on the lattice model.²³ RRDA takes into account the charge-density fluctuation (CDF) effect beyond the mean field and satisfies the microscopic conservation laws.²⁴ For an electron system with long-range Coulomb interactions, CDF is the predominant contribution to

the self-energy of electrons. It has been proved that the RRDA results for the ground-state energy of two- and three-dimensional interacting electron gases are more accurate than the random-phase approximation (RPA) when compared with Monte Carlo simulations.²⁵

In RRDA, the Green's function and self-energy are self-consistently determined by coupled integral equations. There are convolutions of functions in momentum space involved in the calculation of self-energy. These convolutions need to be carried out again and again during the iterations in solving the integral equations. For simplifying the numerical calculation, one usually converts the convolution in momentum space to simple multiplication in real space by Fourier transform. To do so, we need to adopt the lattice model instead of the continuous model. Since the continuous model is the low-energy limiting case of the lattice model, the momentum of the electrons is confined within two circles around the Dirac points.^{26,27} Thus, an abruptly discontinuity because of the momentum cutoff is artificially introduced into the functions, and the conversion of the convolution from momentum space to real space is no longer valid anymore in the simplified continuous model.

The key problem in calculating the self-energy is how to accurately deal with the long-range Coulomb interaction between electrons. For the two-dimensional system under consideration, the interaction is inversely proportional to the momentum transfer q in the long-wavelength limit. In a continuous model, one can transform the $1/q$ singularity to the logarithmic one after performing the azimuthal integration²⁸ and then get rid of the logarithmic singularity by special treatment. On a lattice model, however, we cannot perform the azimuthal integration analytically and must face to the $1/q$ singularity. Since dealing with the long-range Coulomb interaction is inevitable in the many-body problems, a systematic numerical algorithm is desirable. In this work, we will present an effective method for solving this problem.

II. LATTICE MODEL

The lattice structure of bilayer graphene is shown in Fig. 1. The unit cell in each layer is denoted as a diamond. The unit cell of the bilayer system contains four atoms denoted as a_1 , b_1 , a_2 and b_2 . The lattice constant of monolayer graphene is defined as the distance between two nearest corner atoms in the diamond and is given by $a \approx 2.4 \text{ \AA}$. The interlayer distance is $z_0 = 3.34 \text{ \AA} \approx 1.4a$. The energy of electron hopping between the nearest-neighbor (nn) carbon atoms in each layer is $t \approx 2.82 \text{ eV}$,²⁹ while the interlayer nn hopping is $t_1 \approx 0.39 \text{ eV}$.³⁰

The Hamiltonian describing the electrons is given by

$$H = - \sum_{ij\sigma} t_{ij} c_{i\sigma}^\dagger c_{j\sigma} + \frac{1}{2} \sum_{ij} \delta n_i v_{ij} \delta n_j \quad (1)$$

where $c_{i\sigma}^\dagger$ creates an electron at site i with spin σ , $\delta n_j = n_j - n$ with n_j as the electron density operator at site j and n the average occupation number of electrons per site (which is also the charge number of the neutralizing background), v_{ij} is the Coulomb interaction between electrons at sites i and j . The model is restricted to nn hopping within the same layer and between the adjacent sites on top and back layers as shown in Fig. 1. As described by Eq. (1), we here consider only the charge-charge interactions. Since the long-range antiferromagnetic order is prohibited in the two-dimension, and the antiferromagnetic coupling caused by the on-site repulsion is supposed to be weak in our system, we shall neglect the antiferromagnetic coupling in the present work.

We here consider the behavior of Coulomb interaction v_{ij} . At long distance r_{ij} between two electrons at sites i and j , v_{ij} is given by $v_{ij} = e^2/\epsilon r_{ij}$ with ϵ the dielectric constant of high frequency limit of the system. However, at short distance, because of the spreading of π -orbital wavefunction of the conducting electrons, v_{ij} is weakened from the behavior $1/r_{ij}$. Taking the wavefunction spreading effect into account, we model the interaction as

$$v_{ij} = \frac{e^2}{\epsilon r_{ij}} [1 - \exp(-r_{ij}/r_0)] \quad (2)$$

with $r_0 = a$. Clearly, v_{ij} behaves as $e^2/\epsilon r_{ij}$ at large r_{ij} , while it is suppressed from the ‘bare’ Coulomb interaction ($e^2/\epsilon r_{ij}$) at small r_{ij} . Especially, at $r_{ij} = 0$, it is given by a finite value $e^2/\epsilon r_0$. For the present electron system with long-range Coulomb interaction, the final result under consideration should not be sensitively depending on the details of the short range behavior of the interaction. We will use the dimensionless constant $g \equiv e^2/\epsilon a t$ to denote the strength of Coulomb coupling. The range $0.4 \leq g < 1.8$ covers various cases³¹ such as BLG placed on substrates or suspended.

The system defined by Eq. (1) satisfies the particle-hole symmetry. To see this, we denote the doped electron

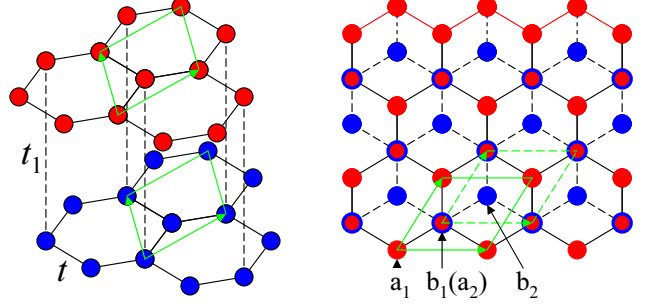


FIG. 1: Left panel: Structure of Bernal stacking bilayer graphene. Right panel: Top view of the bilayer graphene. The parameters t and t_1 are the electron hopping energies between the nearest atoms on the same and different layers, respectively. The unit cell in each layer is denoted as the green-side diamond.

concentration per carbon atom as δ and have $n = 1 + \delta$. Under the transformation $\delta \rightarrow -\delta$ and $c_{j,\sigma} \leftrightarrow \pm c_{j,\sigma}^\dagger$ for electrons at a_j (b_j) site, H is unchanged. Furthermore, $K = H - \mu(\hat{N} - N_0)$ (with \hat{N} the operator of the total number of electrons and N_0 the total number of lattice sites and thereby $N - N_0$ as the total number of doped electrons) is also unchanged under the above transformation and $\mu \rightarrow -\mu$. Thus, the chemical potential μ is an odd function of δ .

The Green's function G of the electron system is defined as

$$G(i, j, \tau - \tau') = -\langle T_\tau C_{i\sigma}(\tau) C_{j\sigma}^\dagger(\tau') \rangle \quad (3)$$

where $C_{j\sigma}^\dagger = (c_{a_1 j \sigma}^\dagger, c_{b_1 j \sigma}^\dagger, c_{a_2 j \sigma}^\dagger, c_{b_2 j \sigma}^\dagger)$ with $c_{a_l(b_l) j \sigma}^\dagger$ creating an electron of spin σ at site a_l (b_l) of l th ($= 1, 2$ respectively for top and back) layer of j th unit cell. G is a 4×4 matrix. In the momentum-frequency space, in terms of the self-energy $\Sigma(k, i\omega_\ell)$ (4×4 matrix), G is expressed as

$$G(k, i\omega_\ell) = [i\omega_\ell + \mu - h_k - \Sigma(k, i\omega_\ell)]^{-1} \quad (4)$$

with

$$h_k = \begin{pmatrix} 0 & \epsilon_k & 0 & 0 \\ \epsilon_k^* & 0 & -t_1 & 0 \\ 0 & -t_1 & 0 & \epsilon_k \\ 0 & 0 & \epsilon_k^* & 0 \end{pmatrix} \quad (5)$$

where $\omega_\ell = (2\ell + 1)\pi T$ is the fermionic Matsubara frequency with ℓ as integer number and T the temperature, and $\epsilon_k = -t_0[1 + \exp(-ik_x) + \exp(-ik_y)]$. Here μ is the chemical potential and is determined by

$$n = \frac{2T}{N_0} \sum_{k\ell} \text{Tr} G(k, i\omega_\ell) \exp(i\omega_\ell \eta), \quad (6)$$

where the factor 2 stems from the spin degeneracy and η is an infinitesimal small positive constant. To proceed,



FIG. 2: Self-energy by SCHFA or the mean-field approximation. Left panel: Hartree term. Right panel: Fock exchange term. The solid line with an arrow denotes the Green's function. The wavy line is the Coulomb interaction.

we need to make approximation for $\Sigma(k, i\omega_\ell)$. In the following sections, we investigate the possibility of the existence of GBISP using SCHFA and RRDA for the self-energy, respectively.

III. STUDY THE EXISTENCE OF GBISP USING SCHFA

First, we consider the physical meaning of GBISP. It is seen from Fig. 1, suppose the origin is at the middle point of a b_1a_2 bond, when changing each atom at site r_j to $-r_j$, the whole lattice is unchanged. This transformation equals to interchanging the top and back layers and then rotating the lattice by angle π around the b_1a_2 bond. In the normal state, the electron system is unchanged under such a transformation. However, when in the GBISP due to the strong Coulomb interaction, the two layers are no more equivalent and the electrons feel different fields on the two layers. Specifically, there may exist net electronic charge accumulation at each atom. The deviations of the electron concentration from the average n , $(\delta_1, \delta_2, -\delta_2, -\delta_1)$ respectively at the four sites in the unit cell, can be expected in GBISP.

Under the SCHFA or the mean-field approximation, the self-energy is diagrammatically given by Fig. 2. The Hartree term is diagonal, $\Sigma_{\mu\nu}^H = \Delta_\mu \delta_{\mu\nu}$, with

$$\Delta_\mu = \delta_1 u_{\mu 1} + \delta_2 u_{\mu 2} \quad (7)$$

$$u_{\mu 1} = \lim_{q \rightarrow 0} [v_{\mu 1}(q) - v_{\mu 4}(q)] \quad (8)$$

$$u_{\mu 2} = \lim_{q \rightarrow 0} [v_{\mu 2}(q) - v_{\mu 3}(q)] \quad (9)$$

where $v_{\mu\nu}(q)$ (with the subscribes $\mu\nu$ the same as for the Green's function denoting the four a_1, b_1, a_2 and b_2 sublattices) is the Fourier component of Coulomb interaction. In the long-wavelength limit, $v_{\mu\nu}(q)$ behaves like

$$v_{\mu\nu}(q) \rightarrow \frac{2\pi e^2}{S_0 \epsilon Q} \exp(-z_{\mu\nu} Q) + \tilde{v}_{\mu\nu}, \quad q \rightarrow 0 \quad (10)$$

where $S_0 = \sqrt{3}a^2/2$ is the area of the two-dimensional unit cell of monolayer graphene, Q is the magnitude of the vector $\vec{Q} = \hat{M}\vec{q}$ with³³

$$\hat{M} = \begin{pmatrix} 1 & 0 \\ -\frac{1}{\sqrt{3}} & \frac{2}{\sqrt{3}} \end{pmatrix}, \quad (11)$$

the components of \vec{q} are along the non-orthogonal axes of the diamond-shape Brillouin zone, $z_{\mu\nu} = 0$ or z_0 (the distance of the two layers) if $\mu\nu$ denotes the same layer or different layer, and $\tilde{v}_{\mu\nu}$ is the remaining regular part. The q -dependence in Eq. (10) is different from the conventional form because the coordinate axes of the reciprocal honeycomb lattice where \vec{q} is defined are not orthogonal. \vec{Q} is the vector with its two components along two orthogonal axes.³³ The relations $\Delta_1 = -\Delta_4$ and $\Delta_2 = -\Delta_3$ can be easily checked.

The Fock exchange term is given by

$$\Sigma_{\mu\nu}^F(k) = -\frac{1}{M} \sum_q v_{\mu\nu}(q) \tilde{n}_{\mu\nu}(k-q) \quad (12)$$

where $M = N_0/4$ is total number of unit cells in one layer, and $\tilde{n}_{\mu\nu}(k)$ is given as

$$\tilde{n}_{\mu\nu}(k) = T \sum_\ell G_{\mu\nu}(k, i\omega_\ell) \exp(i\omega_\ell \eta) - \delta_{\mu\nu}/2, \quad (13)$$

which corresponds to the distribution function with the extra term $-\delta_{\mu\nu}/2$ stemming from the non-normal order of the electron operators in the interaction. Under the mean-field approximation, the self-energy $\Sigma_{\mu\nu}(k) = \Sigma_{\mu\nu}^H + \Sigma_{\mu\nu}^F(k)$ is independent of the frequency. By diagonalizing the effective Hamiltonian $h_k + \Sigma(k)$, one can explicitly carry out the frequency summation in Eq. (13).

The parameters δ_1 and δ_2 are determined by

$$\delta_1 = \frac{1}{M} \sum_k [\tilde{n}_{11}(k) - \tilde{n}_{44}(k)], \quad (14)$$

$$\delta_2 = \frac{1}{M} \sum_k [\tilde{n}_{22}(k) - \tilde{n}_{33}(k)]. \quad (15)$$

So far, all the components of self-energy and parameters are self-consistently determined by the above equations. The magnitude of δ_1 is larger than that of δ_2 . To see it, consider temporarily the isolated b_1 and a_2 atoms without Coulomb interaction. Since they are bonded with t_1 , the energy of their original degenerated states is split to levels $\pm t_1$. Therefore, the states of the b_1 and a_2 sublattices contribute mostly to the non-interacting energy bands of overall $\pm t_1$ from the zero level. At low temperature, the lower band is occupied while the upper band is empty. On the other hand, the valence and conduction bands close to the zero energy level are composed predominately from the states of a_1 and b_2 sublattices. Under the Coulomb interaction, the atoms on these two sublattices are the first to be affected and have more charge accumulation in the GBISP. δ_1 and δ_2 are not independent, but are correlated through the Green's functions. We can chose δ_1 as the independent order parameter of GBISP.

To determine the GBISP phase boundary that is the relation between the critical temperature T_0 and the carrier doping concentration δ , we expand the self-energy

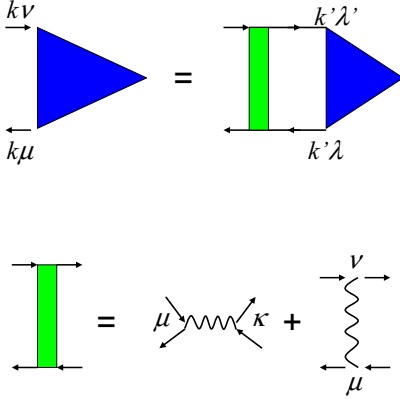


FIG. 3: Equation for particle-hole propagator $D(k)$. Triangle denotes $D(k)$. The effective interaction between particles and holes is obtained by disconnecting a Green's function line in the self-energy given in Fig. 2.

and the Green's function to first order in the order parameter δ_1 . Define the matrix

$$D(k) = \frac{\partial}{\partial \delta_1} [\Sigma(k) - S^\dagger \Sigma^*(k) S] / 2 \quad (16)$$

with

$$S = \begin{pmatrix} 0 & 0 & 0 & 1 \\ 0 & 0 & 1 & 0 \\ 0 & 1 & 0 & 0 \\ 1 & 0 & 0 & 0 \end{pmatrix}. \quad (17)$$

Notice that $\Sigma^*(k) = \Sigma^t(k)$ (the transpose of Σ) since $\Sigma^\dagger(k) = \Sigma(k)$. By this symmetry and the definition, $D(k)$ has the following structure

$$D = \begin{pmatrix} D_{11} & D_{12} & D_{13} & 0 \\ D_{12}^* & D_{22} & 0 & -D_{13} \\ D_{13}^* & 0 & -D_{22} & -D_{12} \\ 0 & -D_{13}^* & -D_{12}^* & -D_{11} \end{pmatrix}. \quad (18)$$

Therefore, only four elements D_{11} , D_{12} , D_{13} and D_{22} need to be determined. Under the mean-field approximation, we have the equation for $D(k)$,

$$D_{\mu\nu}(k) = d_\mu \delta_{\mu\nu} - \frac{1}{M} \sum_{k'\lambda\lambda'} v_{\mu\nu}(k-k') f_{\mu\nu}^{\lambda\lambda'}(k') D_{\lambda\lambda'}(k') \quad (19)$$

with

$$d_\mu = u_{\mu 1} + u_{\mu 2} \frac{\partial \delta_2}{\partial \delta_1} \quad (20)$$

$$f_{\mu\nu}^{\lambda\lambda'}(k) = T \sum_\ell G_{\mu\lambda}(k, i\omega_\ell) G_{\lambda'\mu}(k, i\omega_\ell), \quad (21)$$

where $G(k, i\omega_\ell)$'s are the normal-state Green's functions in which $\delta_1 = \delta_2 = 0$. Again, the frequency summation in

Eq. (21) can be performed analytically. For the normal state, the Green's functions satisfy the relation $G_{\mu\nu} = G_{\bar{\nu}\bar{\mu}}$ with $\bar{\mu} = 5 - \mu$. We therefore have $f_{\mu\nu}^{\lambda\lambda'} = f_{\bar{\nu}\bar{\mu}}^{\bar{\lambda}\bar{\lambda}'}$. By noting these relations, $\partial \delta_2 / \partial \delta_1$ can be expressed as

$$\frac{\partial \delta_2}{\partial \delta_1} = \frac{2}{M} \sum_{k\lambda\lambda'} f_{22}^{\lambda\lambda'}(k) D_{\lambda\lambda'}(k). \quad (22)$$

Taking the partial derivation of Eq. (14) with respect to δ_1 , we obtain the condition for the phase transition,

$$\frac{2}{M} \sum_{k\lambda\lambda'} f_{11}^{\lambda\lambda'}(k) D_{\lambda\lambda'}(k) = 1. \quad (23)$$

Note that d_μ can be formally expressed as

$$\begin{aligned} d_\mu &= \frac{2}{M} \sum_{k\lambda\lambda'} [u_{\mu 1} f_{11}^{\lambda\lambda'}(k) + u_{\mu 2} f_{22}^{\lambda\lambda'}(k)] D_{\lambda\lambda'}(k) \\ &= \frac{2}{M} \sum_{k\kappa\lambda\lambda'} v_{\mu\kappa}(0) f_{\kappa\kappa}^{\lambda\lambda'}(k) D_{\lambda\lambda'}(k), \end{aligned}$$

where in the second line, the definition of $u_{\mu 1(2)}$, $f_{\mu\nu}^{\lambda\lambda'} = f_{\bar{\nu}\bar{\mu}}^{\bar{\lambda}\bar{\lambda}'}$ and $D_{\bar{\lambda}\bar{\lambda}'}(k) = -D_{\lambda\lambda'}(k)$ has been used. (The factor 2 originates from the spin degeneracy.) Putting this result into Eq. (19), one obtains the coupled linear equations for D 's. The equations are diagrammatically shown in Fig. 3. The function $D(k)$ actually is the particle-hole propagator. The effective interaction between particles and holes is the result of disconnecting a Green's function in the self-energy as given by Fig. 2. Clearly, these equations are equivalent to solving the problem of particle-hole propagator with the unity eigen value.

Instead of solving the eigen value equations as given in Fig. 3, $D(k)$'s can be determined much easier from Eqs. (19), (20) and (22) by iterations. For a given carrier doping concentration δ , the transition temperature T_0 can be found by gradually lowering transition temperature T from higher one and solving the equations for D 's in the normal state at each step of the process. With checking the value given by the left band side of Eq. (23), T_0 is reached when the value becomes unity.

To numerically solve the above equations, we need to carefully treat the convolution of the Coulomb interaction $v_{\mu\nu}(q)$ and the function $\tilde{n}_{\mu\nu}(k-q)$ as appeared in Eqs. (12) [and the similar one appeared in Eq. (19)] because $v_{\mu\nu}(q)$ is singular at $q=0$. In Appendix A, we present an algorithm to deal with this problem.

In Fig. 4, we show the phase diagram of the electron system in the $\delta - T$ plane for coupling constant $g = 1$. At low temperature and low carrier doping concentration, the system is in GBISP. The transition temperature as a function of δ is uniquely defined only at low $\delta < 0.24 \times 10^{-4}$. However, in the region $0.24 \times 10^{-4} < \delta < 0.3 \times 10^{-4}$, one δ corresponds to two transition temperatures. In the latter case, the phase boundary was determined by adjusting δ for a given T .

The numerical results for the order parameters δ_1 and δ_2 as functions of T at $\delta = 0$ for coupling constants

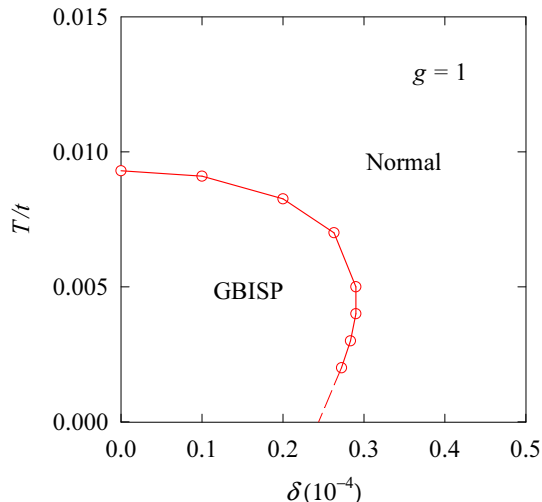


FIG. 4: Phase diagram by SCHFA for coupling constant $g = 1$. The symbols are the numerical solution for transition points. The dashed line is an extrapolation of the finite-temperature results to low temperature.

$g = 0.5, 1$ and 1.8 are shown in Fig. 5. The SCHFA results are denoted as HF. We notice that $|\delta_1| > |\delta_2|$, but δ_2 is not negligible small, this is different from what has been assumed in the two-band model.⁵ From Fig. 5, it is known that the charge configuration at the four sites in the unit cell is $(-|\delta_1|, |\delta_2|, -|\delta_2|, |\delta_1|)$ [another solution is $(|\delta_1|, -|\delta_2|, |\delta_2|, -|\delta_1|)$]. The signs of δ_1 and δ_2 are opposite from each other because by such a charge distribution the Coulomb interaction between the a and b sites in the same plane is attractive and stabilizes the GBISP. It is also seen from Fig.5 that the transition temperature is higher for system with stronger coupling.

The lattice model here is different from both the continuous and two-band models.^{5,9,26,27} The continuous and two-band models are established under the consideration that the energy scale of quasiparticles involved in the problem is small. For the continuous model, the energy should be much less than the band width. The two-band model for BLG applies only to the case of where the energy of quasiparticle is much less than the overall gap t_1 . In the presence of long-range Coulomb interaction $v(q)$, the energy transfer at small q is very large and the assumption for the validity of the continuous and two-band models becomes problematic. In this sense, the lattice model appears to be reasonable.

Another important difference between the lattice model and the continuous two-band model is about the valley physics in the Brillouin zone. In the latter model, the two valleys are independent from each other and are treated as a degree of freedom. However, in the lattice model, they are connected by the energy band and there is no such valley degree of freedom.

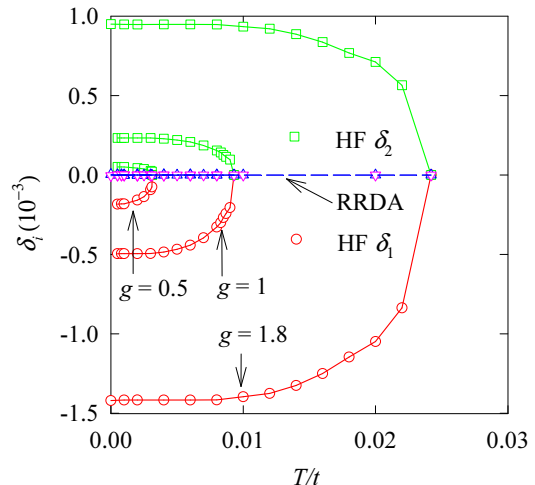


FIG. 5: Order parameters δ_1 and δ_2 as functions of temperature T at $\delta = 0$ for coupling constants $g = 0.5, 1$ and 1.8 . The symbols are the numerical calculations. Circles and squares denoted as HF are the SCHFA results for δ_1 and δ_2 , respectively. The RRDA results denoted by triangles (δ_1) and inverse triangles (δ_2) are vanishing small.

IV. SUPPRESSION OF GBISP IN RRDA

The order parameters δ_1 and δ_2 so obtained by SCHFA are overestimated because charge fluctuations have been ignored. We here reexamine the possibility of the existence of GBISP using RRDA.

Under RRDA, besides the Hartree-Fock terms given in Fig. 2, the additional part of the self-energy, denoted by $\Sigma^c(k, i\omega_\ell)$, is shown in Fig. 6. Each bubble in Fig. 6 is composed by two Green's function G 's, representing the charge polarizability. In terms of G , the elements of $\Sigma^c(k, i\omega_\ell)$ are expressed as

$$\Sigma_{\mu\nu}^c(k, i\omega_\ell) = -\frac{T}{M} \sum_{q,m} G_{\mu\nu}(k-q, i\omega_\ell - i\nu_m) W_{\mu\nu}^c(q, i\nu_m)$$

where ν_m is the bosonic Matsubara frequency, and $W_{\mu\nu}^c(q, i\nu_m)$ is an effective interaction. The matrix form of W^c is given by

$$W^c(q, i\nu_m) = [1 - v(q)\chi(q, i\nu_m)]^{-1}v(q) - v(q) \quad (24)$$

with

$$\chi_{\mu\nu}(q, i\nu_m) = \frac{2T}{M} \sum_{k,\ell} G_{\mu\nu}(k, i\omega_\ell) G_{\nu\mu}(k-q, i\omega_\ell - i\nu_m)$$

and $v(q)$ is the Fourier component (4×4 matrix) of the Coulomb interaction. The total self-energy is given by

$$\Sigma_{\mu\nu}(k, i\omega_\ell) = \Delta_\mu \delta_{\mu\nu} + \Sigma_{\mu\nu}^F(k) + \Sigma_{\mu\nu}^c(k, i\omega_\ell). \quad (25)$$

The Green's function G is self-consistently determined and satisfies the microscopic conservation laws.²⁴



FIG. 6: Additional part of the self-energy besides the Hartree-Fock terms.

Note that Σ^c is a convolution of G and W^c , and χ a convolution of two G 's in momentum and frequency space. The easy way to calculate them is by Fourier transform. At low temperature, the summations over the Matsubara frequency should run to a big cutoff number. For reducing the requirement of the computer memory storage and accelerating the numerical computation, the special algorithm given in Ref. 25 is useable.

The interaction $W^c(q, i\nu_m)$ vanishes in $m \rightarrow \infty$. For finite ν_m , we need to carefully deal with the singularity at $q = 0$. The Fourier transform $W^c(q, i\nu_m)$ to $W^c(r, i\nu_m)$ is discussed in Appendix B.

At the ground states, $T = 0$, the Matsubara frequencies ω_ℓ and ν_m are treated as respectively the continuous variables ω and ν and the summations over them are replaced by integrals,

$$T \sum_{\omega_\ell} \rightarrow \int_{-\infty}^{\infty} \frac{d\omega}{2\pi}$$

$$T \sum_{\nu_m} \rightarrow \int_{-\infty}^{\infty} \frac{d\nu}{2\pi}.$$

We have solved the Green's function under RRDA. The results for the order parameters δ_1 and δ_2 for $g = 0.5, 1$ and 1.8 at $\delta = 0$ are shown in Fig. 5 and compared with the SCHFA. The doping concentration is chosen as $\delta = 0$ for which the SCHFA transition temperature reaches its maximum. Though $\delta = 0$ is the most favorable case for GBISP predicted by SCHFA, the two order parameters are substantially suppressed by CDF in RRDA; the magnitude of the two parameters are three orders smaller than that of SCHFA. For inspecting the GBISP ordering at low temperature, the RRDA calculation for $g = 1.8$ is performed down to $T = 0$. From the numerical results, we conclude that there is no GBISP in systems of $g \leq 1.8$ under RRDA.

We have also calculated the Green's function using the RPA exchange interaction for which the polarizability $\chi(q, i\nu_m)$ in $W^c(q, i\nu_m)$ [see Eq. (24)] is replaced by the one of non-interacting electrons. At $\delta = 0$, similarly as RRDA, the parameters δ_1 and δ_2 so obtained are vanishing small.

The reason for the suppression of GBISP under RRDA is that the exchange interaction is significantly weakened by the screening due to electronic charge-density fluctuations. At low temperature, in a wide range of the Matsubara frequency, the exchange interaction is short-ranged and weakened and does not favor the GBISP transition. We would point out that the suppression of

GBISP here is not due to the prohibition by the Mermin-Wagner theorem.³² The theorem applies to the system with continuous symmetry; if the symmetry were broken, there would be a logarithmically diverging number of long-wavelength collective fluctuations accompanying the broken symmetry in the two-dimensional system. In the present case, the inversion symmetry is the one under discrete transformation and there is no diverging long-wavelength collective fluctuations arising from such a broken symmetry.

V. SUMMARY

In summary, we have studied the physics of interacting electrons in bilayer graphene using the lattice model. The possibility of the existence of GBISP at low temperature and low carrier doping concentration is reinvestigated with both SCHFA and RRDA. The latter approach takes into account the charge-density fluctuations beyond the SCHFA or the mean field approximation. Under RRDA, the exchange interaction is weakened substantially and the existence of GBISP becomes unsustainable. We have also presented the numerical method for dealing with convolution of singular Coulomb interaction and the Green's function on the lattice model. This numerical method should be useable for solving problems in many-particle systems.

Acknowledgments

This work was supported by the National Basic Research 973 Program of China under Grants No. 2012CB932300 and No. 2011CB932700, NSFC under Grant No. 10834011, and the Robert A. Welch Foundation under Grant No. E-1146.

Appendix A: Calculation of the momentum-space convolution of Coulomb interaction with a smooth function for a lattice model

For solving problems of two-dimensional electron system in the presence of long-range Coulomb interaction, we sometimes need to deal with the convolution

$$C(k) = \frac{1}{M} \sum_q V(q) f(k - q) \quad (26)$$

where the q -summation runs over the first Brillouin zone, $V(q)$ is the Coulomb interaction, and $f(k)$ is a smooth function of k . On a lattice, analytical expression for $V(q)$ is not available but its long-wavelength behavior is known. For the honeycomb lattice, it is given by Eq. (10). $V(q)$ can be divided into long-range and short-range parts. For the honeycomb lattice under consideration, define

$$v^l(q) = \sum_n \frac{c}{|\vec{Q}_n + \vec{Q}|} \exp(-a_0 |\vec{Q}_n + \vec{Q}|) \quad (27)$$

where $c = 2\pi e^2/S_0\epsilon$ is the same factor appeared in Eq. (10), \vec{Q}_n is the reciprocal lattice vector, $\vec{Q} = \hat{M}\vec{q}$ as given in the text, and a_0 is an auxiliary parameter. By taking $a_0 = 2a$, the summation in Eq. (27) converges fast and only a few terms need to be summed up. Clearly, $v^l(q)$ represents a long-range interaction. With $v^l(q)$, $v(q)$ can be written as

$$V(q) = v^l(q) + v^s(q) \quad (28)$$

where $v^s(q)$ is so defined by the equation and is the short-range part of $V(q)$. Note that both $v^l(q)$ and $v^s(q)$ are periodic functions of q . Equation (26) now is given by

$$C(k) = \frac{1}{M} \sum_q v^s(q) f(k-q) + \frac{1}{M} \sum_q v^l(q) f(k-q) \quad (29)$$

The first integral in Eq. (29) can be safely performed by Fourier transform. In the second integral, the singularity appears at $q = 0$. To find out an auxiliary function for this integral, we pay attention to the expanding form of $f(k-q)$

$$f(k-q) \rightarrow f(k) - q_x f_x(k) - q_y f_y(k) \quad (30)$$

where $f_{x(y)}(k) = df(k)/dk_{x(y)}$. Define two auxiliary functions $v_x(q)$ and $v_y(q)$ by

$$v_{x(y)}(q) = \sum_n \frac{c[q_{x(y)} + (\hat{M}^{-1}\vec{Q}_n)_{x(y)}]}{|\vec{Q}_n + \vec{Q}|} \exp(-a_0|\vec{Q}_n + \vec{Q}|).$$

$v_{x(y)}(q)$ is periodic and odd under $\vec{q} \rightarrow -\vec{q}$. The second integral in Eq. (29) can be written as

$$\begin{aligned} \frac{1}{M} \sum_q v^l(q) f(k-q) &= \frac{1}{M} \sum_{k'} \{v^l(k-k')[f(k') - f(k)] \\ &\quad + v_x(k-k')f_x(k) \\ &\quad + v_y(k-k')f_y(k)\} \\ &\quad + f(k)v^l(r)|_{r=0}. \end{aligned} \quad (31)$$

Now, there is no singularity in the integrand in Eq. (31). The leading term of $v^l(k-k')[f(k') - f(k)]$ as $k' \rightarrow k$ is proportional to the derivative of f multiplied with a sign factor since $v^l(k-k') \propto 1/|\hat{M}(\vec{k}' - \vec{k})|$. This leading term varies discontinuously at $k' = k$. The discontinuity is cancelled out by the remaining term $v_x(k-k')f_x(k) + v_y(k-k')f_y(k)$. As a result, the integrand is a smooth function. The integral can then be carried out numerically. The last term stems from the introduction of the auxiliary functions to the integrand. The value $v^l(r)|_{r=0}$ is given by

$$v^l(r)|_{r=0} = \frac{1}{M} \sum_q v^l(q), \quad (32)$$

which can be calculated explicitly. Replace q -summation by

$$\frac{1}{M} \sum_q \rightarrow \frac{S_0}{V} \sum_Q = S_0 \int_{\text{BZ}} \frac{d\vec{Q}}{(2\pi)^2} \quad (33)$$

where $S_0 = \sqrt{3}a^2/2$ is the area of the unit cell of honeycomb lattice as appeared in the text, BZ means the integral is performed over the first Brillouin zone. The combination of the integration over BZ and the Q_n -summation in the definition of $v^l(q)$ equals to the integration of the function $c \exp(-a_0Q)/Q$ over the total space of Q ,

$$\begin{aligned} v^l(r)|_{r=0} &= S_0 \int \frac{d\vec{Q}}{(2\pi)^2} \frac{c}{Q} \exp(-a_0Q) \\ &= e^2/a_0. \end{aligned} \quad (34)$$

The function $f(k)$ is assumed to be smooth here. However, for calculating the Fock exchange self-energy, $f(k)$ corresponds to the distribution function and varies dramatically at the Fermi surface at low temperature. In this case, much dense grids in a momentum regime covering the Fermi surface should be used to denote the variation of $f(k)$.

The term $v_x(k-k')f_x(k) + v_y(k-k')f_y(k)$ was introduced in right hand side of Eq. (31) in order to smooth the integrand. Because $v_x(q)$ and $v_y(q)$ are periodic and odd functions of q , the contribution from integral of $v_x(k-k')f_x(k) + v_y(k-k')f_y(k)$ is zero. At $T = 0$, there is a discontinuity in $f(k)$ at the Fermi surface and its derivatives $f_x(k)$ and $f_y(k)$ are delta functions. Therefore, the use of this term at $T = 0$ is unworthy. At $T = 0$, this term should be removed, keeping the discontinuity in the integrand. The pay is to use dense grids near the Fermi surface to ensure the accuracy of the result.

Appendix B: Fourier transform of the screening potential $W^c(q, i\nu_m)$

To take the Fourier transform of $W^c(q, i\nu_m)$ given by Eq. (24) from momentum space to real space, we firstly pay attention to its singularity at $q = 0$. For small ν_m , because $\chi(q, i\nu_m)$ is finite, the singularity exists only in the second term $v(q)$ in right hand side of Eq. (2). Its real space form is known as given by Eq. (2) for its elements. However, at large ν_m , because $\chi(q, i\nu_m)$ is vanishing small, there is also a singularity in the first term in right hand side of Eq. (2) and both terms cancel with each other. We need a systematic numerical scheme for the Fourier transform at any ν_m .

Note that in the limit $q \rightarrow 0$ $v(q) \rightarrow v_0(q)\hat{A}$ with $v_0(q) = c/Q$ (again $c = 2\pi e^2/S_0\epsilon$ and $Q = |\hat{M}\vec{q}|$) and

$$\hat{A} = \begin{pmatrix} 1 & 1 & 1 & 1 \\ 1 & 1 & 1 & 1 \\ 1 & 1 & 1 & 1 \\ 1 & 1 & 1 & 1 \end{pmatrix}.$$

In the same limit, we have

$$\begin{aligned} W^c(q, i\nu_m) &\rightarrow -\frac{\alpha_m c}{Q(Q + \alpha_m)} \hat{A} \\ &= W_m(Q)\hat{A}, \end{aligned} \quad (35)$$

with

$$\alpha_m = -c \sum_{\mu\nu} \chi_{\mu\nu}(0, i\nu_m) \quad (36)$$

and $W_m(Q)$ so defined by Eq. (35). By observing this asymptotic form, we take the auxiliary function for the Fourier transform as

$$W_a(q) = \sum_n W_m(|\vec{Q} + \vec{Q}_n|) \exp(-a_0|\vec{Q} + \vec{Q}_n|) \quad (37)$$

where a_0 again is a parameter for fast converging of the summation over the reciprocal lattice vectors \vec{Q}_n . The Fourier transform of $W^c(q, i\nu_m)$ is separated to two parts, $[W^c(q, i\nu_m) - W_a(q)\hat{A}]$ and $W_a(q)\hat{A}$. There is no singularity in the first one and it can be safely transformed by numerical computation. For the second one, $W_a(q)$ is transformed as

$$\begin{aligned} W_a(r) &= a^2 \int_{BZ} \frac{d\vec{q}}{(2\pi)^2} W_a(q) \exp(i\vec{q} \cdot \vec{r}) \\ &= S_0 \int_{BZ} \frac{d\vec{Q}}{(2\pi)^2} W_a(q) \exp(i\vec{Q} \cdot \vec{R}) \\ &= S_0 \int \frac{d\vec{Q}}{(2\pi)^2} W_m(Q) \exp(i\vec{Q} \cdot \vec{R}) \\ &= -\frac{S_0 \alpha_m c}{2\pi} \int_0^\infty dQ \frac{\exp(-a_0 Q)}{Q + \alpha_m} J_0(QR) \quad (38) \end{aligned}$$

where the first line is the definition with \vec{q} and \vec{r} given in the quadrilateral coordinate system, the second line converts \vec{q} to $\vec{Q} = \hat{M}\vec{q}$ and $\vec{R} = \hat{M}^{-1}\vec{r}$ in the orthogonal systems with $d\vec{q} = d\vec{Q}/|\hat{M}| = \sqrt{3}d\vec{Q}/2$, the third line comes from the definition of $W_a(q)$ given by Eq. (37), the last line is obtained after the azimuthal integration, and $J_0(QR)$ is the Bessel function. Now the singularity in the integrand exists only when $\alpha_m = 0$, but α_m also appears in the front factor and the integral vanishes. However, for large R , $J_0(QR)$ oscillates rapidly with Q . By observing the large- QR behavior of $J_0(QR)$, we choose the auxiliary function²⁸

$$\begin{aligned} J_A(z) &= \sqrt{\frac{1}{\pi z + 1}} \left\{ \left[1 + \frac{\pi^2 z}{8(\pi z + 1)^2} \right] \sin(z) \right. \\ &\quad \left. + \left[1 - \frac{\pi^2 z}{8(\pi z + 1)^2} \right] \cos(z) \right\} \quad (39) \end{aligned}$$

and separate $J_0(QR)$ to $[J_0(QR) - J_A(QR)]$ and $J_A(QR)$. By replacing $J_0(QR)$ with $[J_0(QR) - J_A(QR)]$ in Eq. (38), the integral can be accurately carried out by simple numerical method. The remaining integral with $J_0(QR)$ replaced by $J_A(QR)$ can be performed using the Filon's method.

-
- ¹ T. Ohta, A. Bostwick, T. Seyller, K. Horn, E. Rotenberg, *Science* **313**, 951 (2006).
- ² J. B. Oostinga, H. B. Heersche, X. Liu, A. F. Morpurgo, and L. M. K. Vanderspen, *Nature Mater.* **7**, 151 (2008).
- ³ E. McCann, *Phys. Rev. B* **74**, 161403(R) (2006).
- ⁴ E. V. Castro, K. S. Novoselov, S. V. Morozov, N. M. R. Peres, J. M. B. Lopes dos Santos, J. Nilsson, F. Guinea, A. K. Geim, and A. H. Castro Neto, *Phys. Rev. Lett.* **99**, 216802 (2007).
- ⁵ H. K. Min, G. Borghi, M. Polini, and A. H. MacDonald, *Phys. Rev. B* **77**, 041407(R) (2008).
- ⁶ R. Nandkishore and L. Levitov, *Phys. Rev. Lett.* **104**, 156803 (2010).
- ⁷ F. Zhang, H. K. Min, M. Polini, and A. H. MacDonald, *Phys. Rev. B* **81**, 041402(R) (2010).
- ⁸ J. Jung, F. Zhang, and A. H. MacDonald, *Phys. Rev. B* **83**, 115408 (2011).
- ⁹ A. H. MacDonald, J. Jung, and F. Zhang, *Phys. Scr.* **T146**, 014012 (2012).
- ¹⁰ M. Kharitonov, arXiv:1109.1553.
- ¹¹ O. Vafek, *Phys. Rev. B* **82**, 205106 (2010).
- ¹² R. Nandkishore and L. Levitov, *Phys. Rev. B* **82**, 115124 (2010).
- ¹³ F. Zhang, J. Jung, G. A. Fiete, Q. Niu, and A. H. MacDonald, *Phys. Rev. Lett.* **106**, 156801 (2011).
- ¹⁴ F. Zhang and A. H. MacDonald, *Phys. Rev. Lett.* **108**, 186804 (2012).
- ¹⁵ H. Dahal, T. Wehling, K. Bedell, J. Zhu, and A. V. Balatsky, *Physica.* **405**, 2241 (2010).
- ¹⁶ O. Vafek, and K. Yang, *Phys. Rev. B* **81**, 041401 (2010).
- ¹⁷ Y. Lemonik, I. L. Aleiner, C. Toke, and V. I. Fal'ko, *Phys. Rev. B* **82**, 201408(R) (2010).
- ¹⁸ R. T. Weitz, M. T. Allen, B. E. Feldman, J. Martin, and A. Yacoby, *Science* **330**, 812 (2010).
- ¹⁹ F. Freitag, J. Trboćiv, M. Weiss, and C. Schüenberger, *Phys. Rev. Lett.* **108**, 076602 (2012).
- ²⁰ J. Velasco Jr., L. Jing, W. Bao, Y. Lee, P. Kratz, V. Aji, M. Bockrath, C. N. Lau, C. Varma, R. Stillwell, D. Smirnov, F. Zhang, J. Jung, and A. H. MacDonald, *Nature Nanotech.* **7**, 156 (2012).
- ²¹ W. Bao, J. Velasco Jr., L. Jing, F. Zhang, B. Standley, D. Smirnov, M. Bockrath, A. H. MacDonald, and C. N. Lau, arXiv:1202.3212.
- ²² A. S. Mayorov, D. C. Elias, M. Mucha-Kruczynski, R. V. Gorbachev, T. Tudorovskiy, A. Zhukov, S. V. Morozov, M. I. Katsnelson, V. I. Fal'ko, A. K. Geim, and K. S. Novoselov, *Science* **333**, 860 (2011).
- ²³ X. -Z. Yan and C. S. Ting, *Phys. Rev. B* **84**, 035457 (2011).
- ²⁴ G. Baym and L. P. Kadanoff, *Phys. Rev.* **124**, 287 (1961); G. Baym, *Phys. Rev.* **127**, 1391 (1962).
- ²⁵ X. -Z. Yan, *Phys. Rev. E* **84**, 016706 (2011).
- ²⁶ E. McCann and V. I. Fal'ko, *Phys. Rev. Lett.* **96**, 086805 (2006).
- ²⁷ K. S. Novoselov, E. McCann, S. V. Morozov, V. I. Fal'ko, M. I. Katsnelson, U. Zeitler, D. Jiang, F. Schedin, and Geim, *Nat. Phys.* **2**, 177 (2006).

- ²⁸ X.-Z. Yan and C. S. Ting, Phys. Rev. B **75**, 035342 (2007).
- ²⁹ A. Bostwick, T. Ohta, T. Seyller, K. Horn, and E. Rotenberg, Nat. Phys. **3**, 36 (2007).
- ³⁰ A. Misu, E. E. Mendez, and M. S. Dresselhaus, J. Phys. Soc. Jpn. **47**, 199 (1979).
- ³¹ C. Jang, S. Adam, J. -H. Chen, E. D. Williams, S. Das Sarma, and M. S. Fuhrer, Phys. Rev. Lett. **101**, 146805 (2008).
- ³² N. D. Mermin and H. Wagner, Phys. Rev. **17**, 1133 (1966).
- ³³ X.-Z. Yan and C. S. Ting, Phys. Rev. B **76**, 155401 (2007).